Niobium-Containing Structural Steel Developments Meeting Increased Design Application Demands

Dr. S. G. Jansto[1] (Jansto@cbmmna.com) and Wang Houxin[2]

[1]CBMM North America, Inc.,1000 Old Pond Road, Bridgeville, PA 15017, USA
[2]CITIC., 1000 Old Pond Road, Bridgeville, PA 15017, USA

Abstract
Niobium-containing structural steel applications are increasing in global importance as improved mechanical properties are demanded by architects, civil engineers, designers and fabricators. The supply chain is demanding improved fatigue resistance, better fracture toughness, improved formability, less yield-to-tensile ratio variability and better weldability. Increased production of Nb-containing steels has resulted from successful developments in the H-beam, reinforcing bar, pre-stressed concrete wire rod and structural plate markets. The grain refinement benefit is described in conjunction with lower carbon non-peritectic steel metallurgy for H-beam, bridge steels, weathering steels and construction plate steels. The adaptation of Nb in lower carbon rebar demonstrates improved ductility, bendability and high strength reinforcing bar production through the application of thermomechanical processing (TMCP). Another new global development involves the micro-addition of Nb in eutectoid carbon steels for improved drawability and reduced rejects during the production of pre-stressed wire rods for concrete structure. The cost-benefit advantages and attributes of these new Nb-containing structural steel products are discussed.

Keywords:

1. Introduction

The objective of the present paper is to address the attractive nature of niobium in the production of structural beams and plates, with particular focus on the microstructure-property relationship. The objectives of adding niobium to steels are diverse and include: (a) combine with nitrogen content of steels by pinning nitrogen, thereby decreasing the free nitrogen-content for the benefit of toughness [1], (b) prevent austenite recrystallization and/or grain growth during processing [2], (c) control of austenite grain size, (d) lower austenite-ferrite transformation temperature, retarding ferrite formation in microalloyed steels, (e) refine polygonal-ferrite grains during transformation [3], and (f) precipitation hardening [3].

In the production of high strength low alloy steels, several of the above effects may operate simultaneously or individually. The magnitude of each effect varies proportionately with the niobium content and depends on thermo-mechanical processing.

Over 50% of the structural plate and beam sections are intermediate carbon levels from 0.15 to 0.22%. There is a gradual shift at some mills seeking participation in the value added structural plate and beam segment to Nb-bearing structural grades at less than 0.10%C to transition to lower carbon base alloys for both plate and some long product applications. The benefits are not only improved mechanical properties and functional performance, but also the opportunity to reduce overall steelmaking cost per tonne through improved productivity, reduced diverts and improved product quality. [4]

Excellent research and development progress has resulted in the successful commercialization of lower carbon Nb bearing microalloyed plate steel and near net shape cast and rolled beams throughout the world.

Many of these progressive metallurgical accomplishments are presented within this text. With increasing raw material and energy costs, the effects of processing parameters such as reheating temperature and cooling rate after hot rolling to achieve improved mechanical properties can result in significant savings. A lower total cost of production may be achieved through a low carbon-low alloy (LCLA©) chemistry with selective accelerated cooling and better control of reheat furnace temperatures. [4]

The strength is enhanced with the addition of Nb because of the cumulative contribution of refinement in grain size and precipitation of NbC in the ferrite grains. Figure 1 schematically illustrates the effect of niobium addition on grain refinement and increment of yield strength in steels. Niobium offers advantage, via a pinning effect on the austenite grain size and widens the temperature range of austenite processing [4]. Niobium nitrides or carbonitrides impede the coarsening of the austenite grains in a manner similar to aluminum nitrides. This effect is important to ensure a fine microstructure. The sluggish nature of recrystallization in Nb-treated steels, results in pancake-shaped austenite grains leading to significant grain refinement.

The choice of Nb as a microalloying element compared to aluminum, titanium and vanadium is because of the precipitation hardening and refinement of microstructure that gives a combination of high yield strength and toughness; whereas combined microalloying effect with titanium may exhibit a reduced hardening due to interaction of TiN precipitates with Nb [5].

In low carbon bainitic steels, Nb along with Mn and Mo is effective in increasin g the volume fraction of bainite that increases both yield strength and tensile strength. Figure 2 describes the effect of Nb on strength and toughness properties of MoNi-steel plate of 20 mm thickness [6]. In bainitic plates, the primary microstructure is polygonal ferrite and granular bainite while the secondary constituents include martensite and retained austenite. The increase in Nb content was observed to increase granular bainite and refine the second phase constituents.

2. Results and Discussion

2.1. Niobium in Structural Steels

We will now discuss a recent study that describes significant advantages of niobium microalloying in structural beams. Here, we make a comparison between Nb- and V-microalloyed steels processed under similar processing conditions with no intentional differences, where it is shown that both Nb- and V-microalloyed steels exhibited similar yield strength, tensile strength, and ductility. However, impact toughness was significantly higher in Nb-bearing steels. A similar behavior was observed at different cooling rates and has been described recently [7].

The chemical composition range of Nb- and V-microalloyed steels is presented in Table 1. The composition range meets the ASTM specification. It may be noted that the niobium content required to obtain the desired yield strength of 55-60 ksi in structural beams was approximately one-third of the vanadium content.

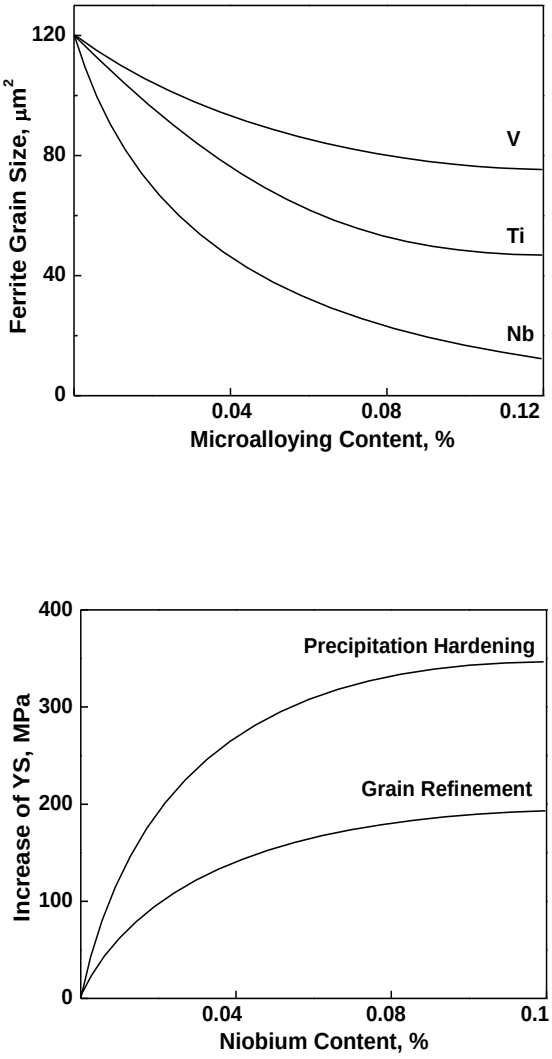

Figure 1. Influence of niobium on grain size and mechanical properties of microalloyed steels [5].

Table 1. Chemical Composition Range of Nb- and V-Microalloyed Steels.

Elements	Nb-microalloyed steel (wt.%)	V-microalloyed steel (wt.%)
C	0.030-0.100	0.030-0.100
Mn	0.500-1.500	0.500-1.500
V	0.001	0.020-0.050
Nb	0.020-0.050	0.001
Si	0.15-0.25	0.15-0.25
P	0.010-0.020	0.010-0.020
S	0.015-0.025	0.015-0.025
N	0.009-0.010	0.009-0.010

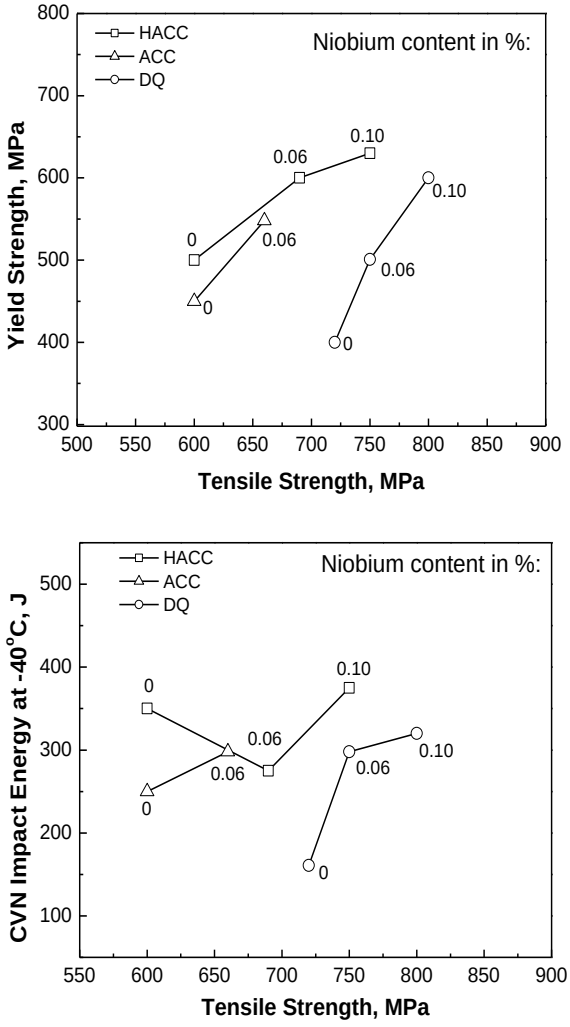

Figure 2. Effect of Nb and cooling on tensile and toughness properties of MoNi-steel plate of 20 mm thickness. (HACC: Heavy Accelerated Cooling, ACC: Accelerated Cooling, DC: Direct Quenching) [6].

Table 2. Representative Room Temperature Tensile Properties of Nb- and V-Microalloyed Steels

Properties	Nb-microalloyed steels	V-microalloyed steels
Yield Strength, ksi	57-60	58-61
Tensile Strength, ksi	72-74	75-76
% Elongation	23-26	23-25

2.2. Tensile and Impact Behavior of Nb- and V-Microalloyed Steels

Tensile property data for Nb- and V-microalloyed steels are listed in Table 2 for conventionally cooled beams. Both the steels exhibited similar yield strength, tensile strength, and percent elongation. A similar behavior was observed at other cooling rates. However, there was variation in toughness of the two steels, as schematically depicted in Figure 3. Figure 3 shows the variation of impact toughness of Nb- and V-microalloyed steels as a function of cooling rate. It may be noted that the steels generally experienced improvement in toughness with increase in cooling rate. However, the toughness improvement was greater in Nb-microalloyed steels as compared to V-microalloyed steels.

2.3. Microstructure of Nb-Microalloyed Steels

Representative low and high magnification scanning electron micrographs of Nb-microalloyed steels processed at different cooling rates are presented in Figures 4-6. The primary microstructural constituents at low cooling rate were polygonal ferrite and pearlite. At intermediate and high cooling rates the microstructure consisted of lath-type/bainitic ferrite, and degenerated pearlite together with conventional ferrite-pearlite. With increase in cooling rate, there was an increased tendency towards formation of lath ferrite/bainitic ferrite with consequent decrease in conventional ferrite-pearlite microstructure. The microstructural transformation from low to intermediate to high cooling rate can be summarized as ferrite-pearlite→ferrite-degenerated pearlite→bainitic ferrite. The average grain size of the steels processed at different cooling rates was similar and in the range of ~ 10-12 μm.

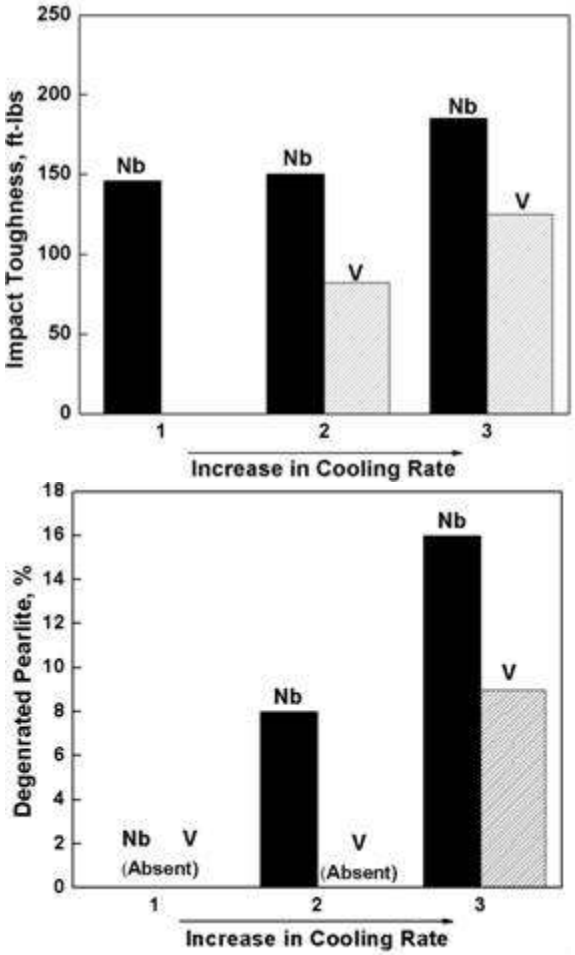

Figure 3. (a) Room temperature Charpy v-notch impact toughness and (b) % degenerated pearlite of Nb- and V-microalloyed steels [6].

In Figures 7-9, representative bright field TEM micrographs of ferrite microstructures of Nb-microalloyed steels processed at low, intermediate and high cooling rates are presented. It can be seen that the steel processed at low cooling rate (Figures 7a-c) contains polygonal ferrite having coarse and fine grain size distribution (Figures 7b-c). At intermediate cooling rate, the microstructure consisted of elongated ferrite grains (Figure 8a) and also some coarse grains with high dislocation density (Figures 8b-c). At high cooling rate the microstructure predominantly contained lath-type or bainitic ferrite (Figures 9a-c). The different type of ferrite morphologies must have formed by a different mechanism [8, 9]. Majority of the ferrite laths are oriented along a particular direction with occasional presence of discontinuous cementite layers between them. If the driving force for the transformation is the reduction in carbon content, then the austenite is most likely to transform to lath-type ferrite by shear mechanism at temperatures greater than 350°C [8].

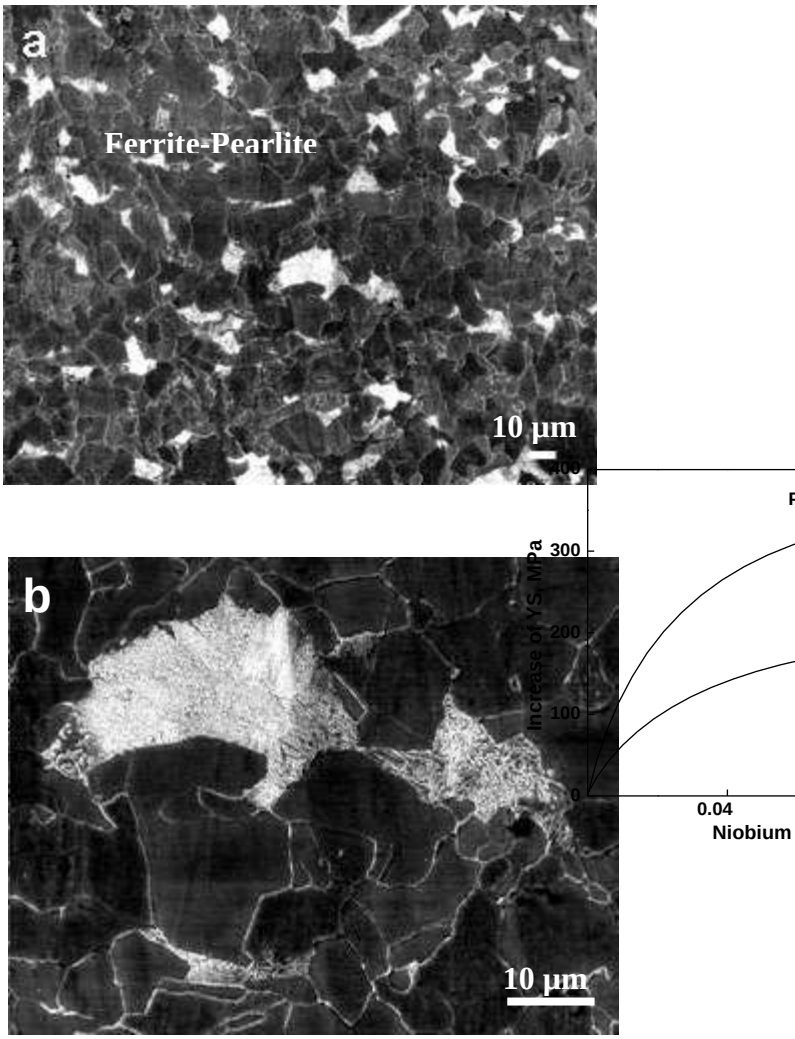

Figure 4. Representative low and high magnification scanning electron micrographs of Nb-microalloyed steels processed at (a, b) low cooling rate.

Representative bright field TEM micrographs of pearlite microstructures of Nb-microalloyed steels processed at low, intermediate and high cooling rates are presented in Figures 10-12, respectively. With increase in cooling rate the cementite morphology in pearlite changed from lamellar pearlite to degenerated pearlite and finally to small cementite particles. The steel processed at low cooling rate (Figures 10a-b) contains lamellar pearlite and broken lamellae (Figure 10c). At intermediate cooling rate some degenerated pearlite is also observed (Figures 11a-b). The SAD pattern analysis of degenerated pearlite (Figure 11b) is presented in Figure 11c. The analysis indicated that the cementite exhibits $[112]_{\alpha}$ //$[122]_{Fe_3C}$ orientation

relationship with ferrite matrix, which is close to 'Pitsch' orientation relationship that is commonly observed in lamellar pearlite.

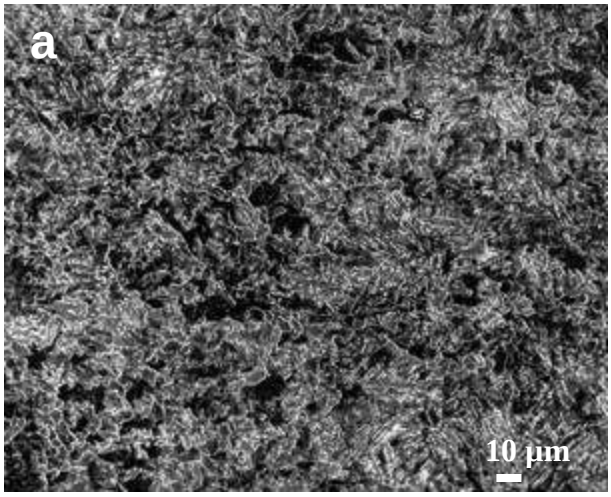

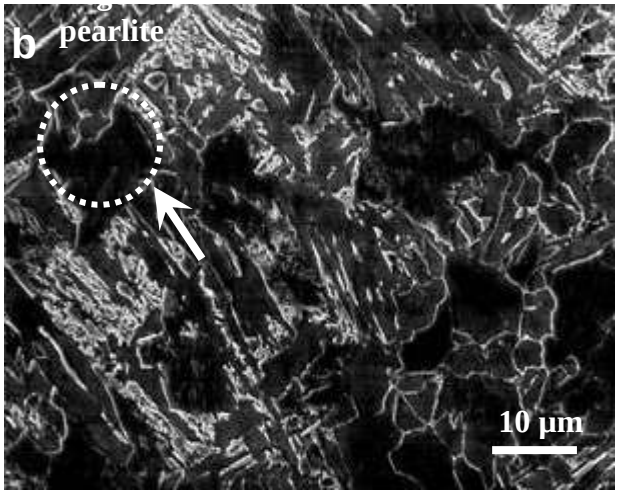

Figure 5. Representative low and high magnification scanning electron micrographs of Nb-microalloyed steels processed at (a, b) intermediate cooling rate. The micrograph (b) shows degenerated pearlite [7].

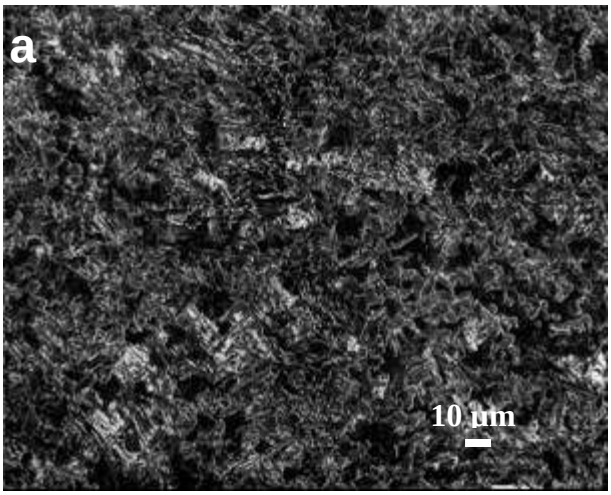

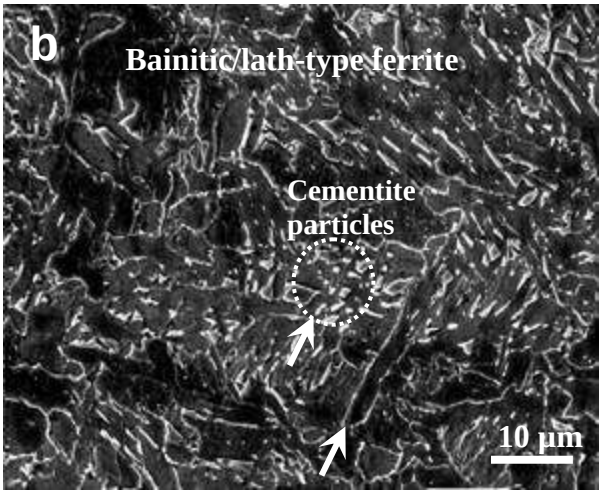

Figure 6. Representative low and high magnification scanning electron micrographs of Nb-microalloyed steels processed at (a, b) high cooling rate [6].

Degenerated pearlite is formed by nucleation of cementite at ferrite/austenite interface followed by carbide-free ferrite layers enclosing the cementite particles in the transformation temperature range between normal pearlite and upper bainite [10]. Similar to lamellar pearlite, degenerated pearlite is also formed by diffusion process and considering its morphology, the difference is attributed to the insufficient carbon diffusion to develop continuous lamellae [8]. It is reported that the interface between ferrite and cementite in degenerated pearlite is wider than the conventional pearlite, thus the ferrite grain boundary area of the controlled-rolled steels that contain degenerated pearlite is higher as compared to the conventionally processed steel [11]. Degenerated pearlite is believed to promote toughness [11].

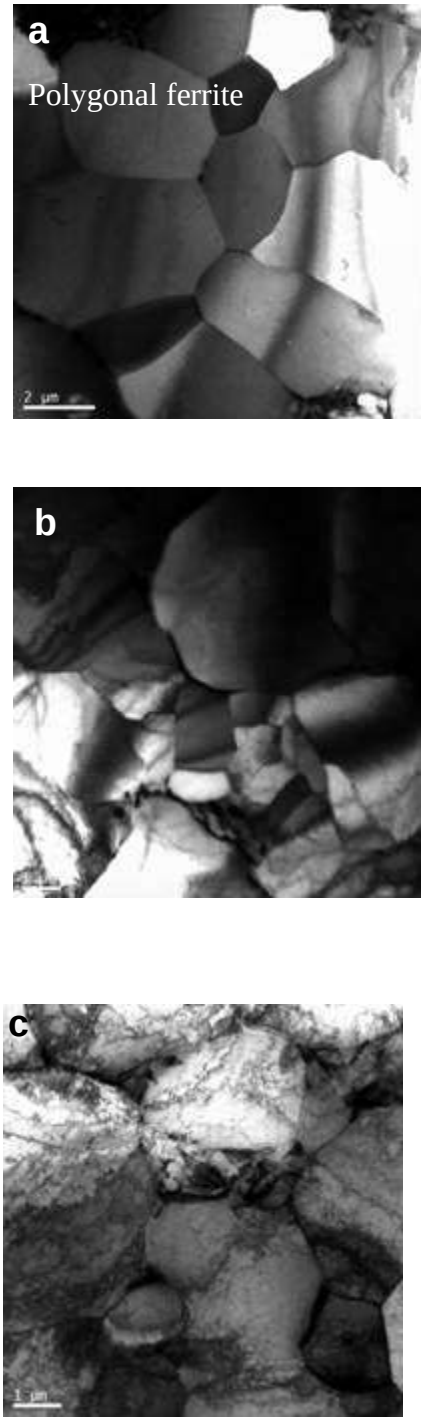

Figure 7. Bright field TEM micrographs of Nb-microalloyed steels processed at low (or normal) cooling rate showing (a, b) polygonal ferrite structure and (c) dislocation substructure in ferrite [7].

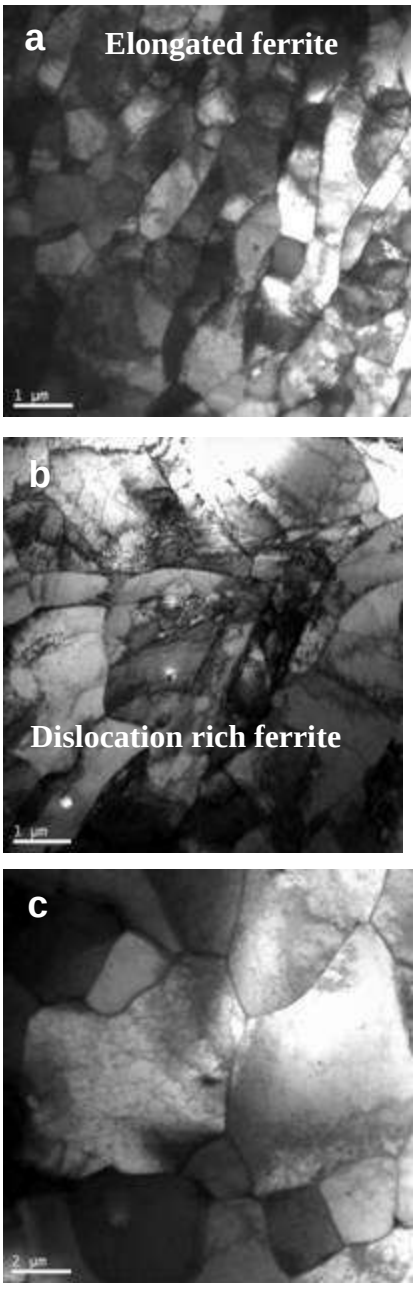

Figure 8. Bright field TEM micrographs of Nb-microalloyed steels processed at intermediate cooling rate showing (a, b) elongated ferrite structure and (c) dislocation substructure in ferrite [7].

At high cooling rate, the microstructure predominantly contained cementite particles dispersed in the ferrite matrix (Figures 12a-b) and at ferrite boundaries (Figure 12c) of size range of ~ 60-120 nm. The driving force for cementite particle formation is the reduction in interfacial area between cementite lamellae and ferrite matrix [12, 13]. The carbon content of ferrite

in equilibrium with cementite is stated be higher at fragmented ends of cementite of large interface curvature than the areas of small interface curvatures. Hence, the spheroidization or formation of small particles is attributed to carbon diffusion through a ferrite matrix from regions of small radius of curvature to regions of large radius of curvature [12, 13].

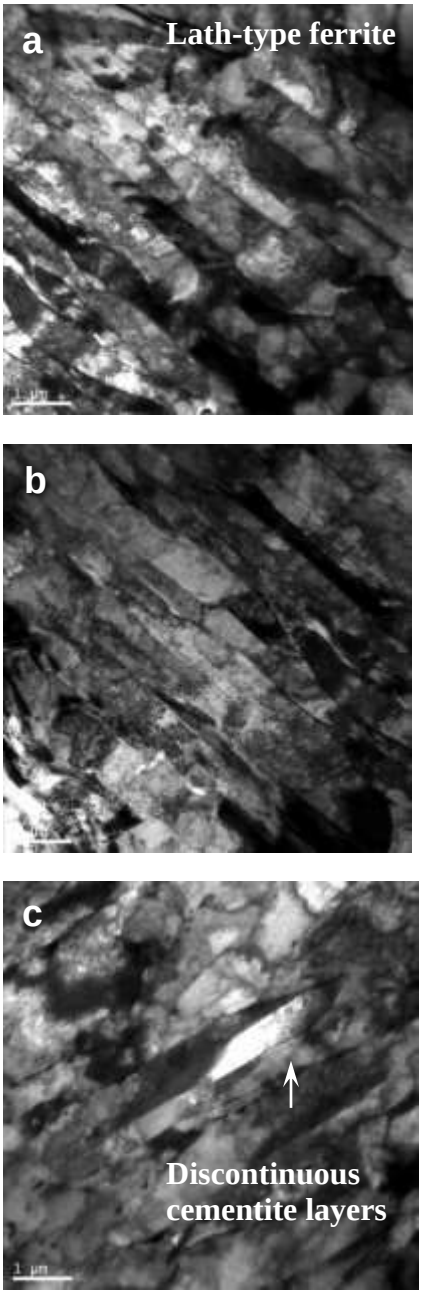

Figure 9. Bright field TEM micrographs of Nb-microalloyed steels processed at high cooling rate showing (a, b and c) bainitic/lath-type ferrite structure [7].

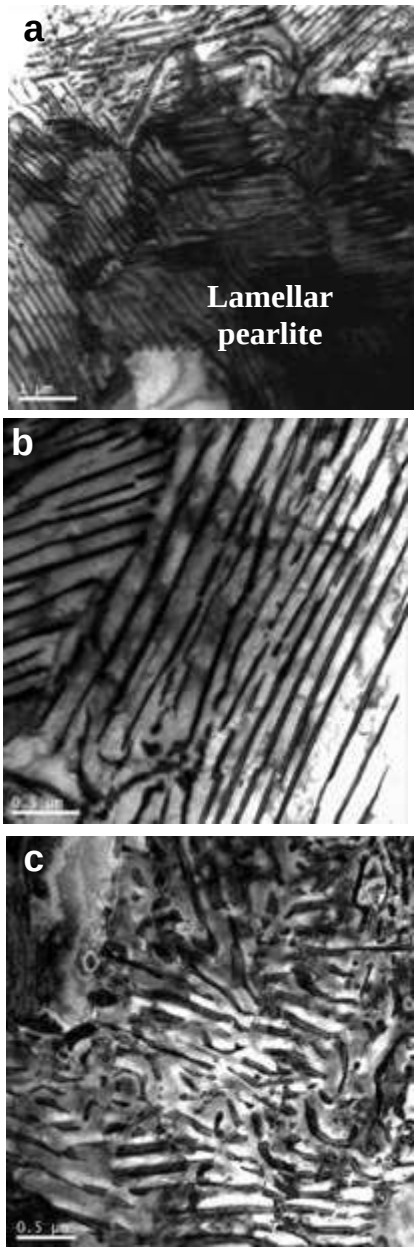

Figure 10. Bright field TEM micrographs of Nb-microalloyed steels processed at low (or normal) cooling rate showing (a, b) lamellar pearlite structure and (c) broken-lamellae pearlite structure [7].

2.4. Microstructure of V-Microalloyed Steels

The micrographs of V-microalloyed steels processed at conventional and high cooling rates are presented in Figures 13 (a,b) and 13 (c,d), respectively. The primary microstructural constituents of V-microalloyed steels processed at conventional and high cooling rates were polygonal ferrite, pearlite, and degenerated pearlite.

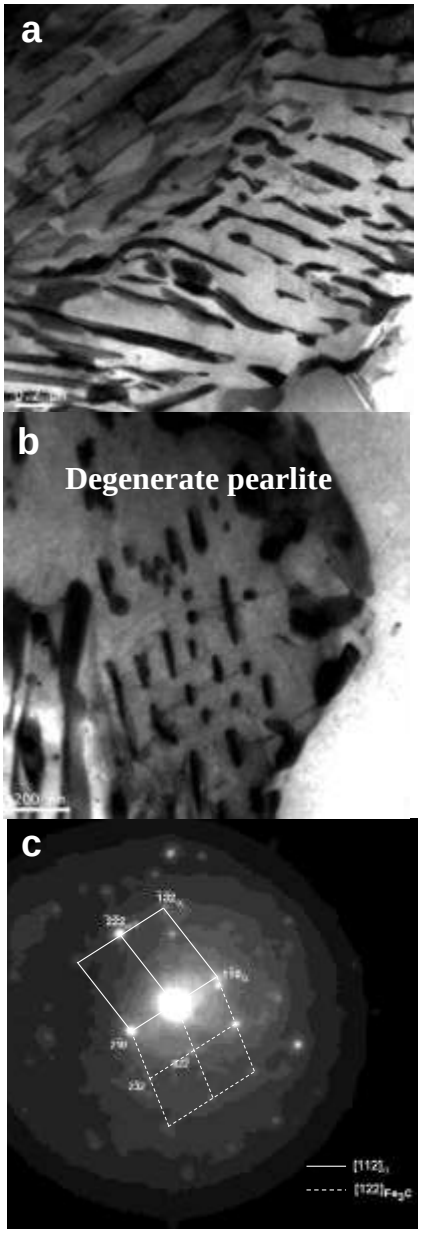

Figure 11. Bright field TEM micrographs of Nb-microalloyed steels processed at intermediate cooling rate showing (a, b) degenerated pearlite structure and (c) SAD pattern analysis for image (b) [7].

Figures 14a and 14b show the general microstructure and dislocation density in ferrite, of V-microalloyed steels. The microstructures of V-microalloyed steels that contained polygonal ferrite, lath-type ferrite grain structure and degenerated pearlite are presented in Figure 15. At higher cooling rates, it is anticipated that the austenite transforms to fine ferrite crystals in the intermediate temperature range as compared to the conventional ferrite structure.

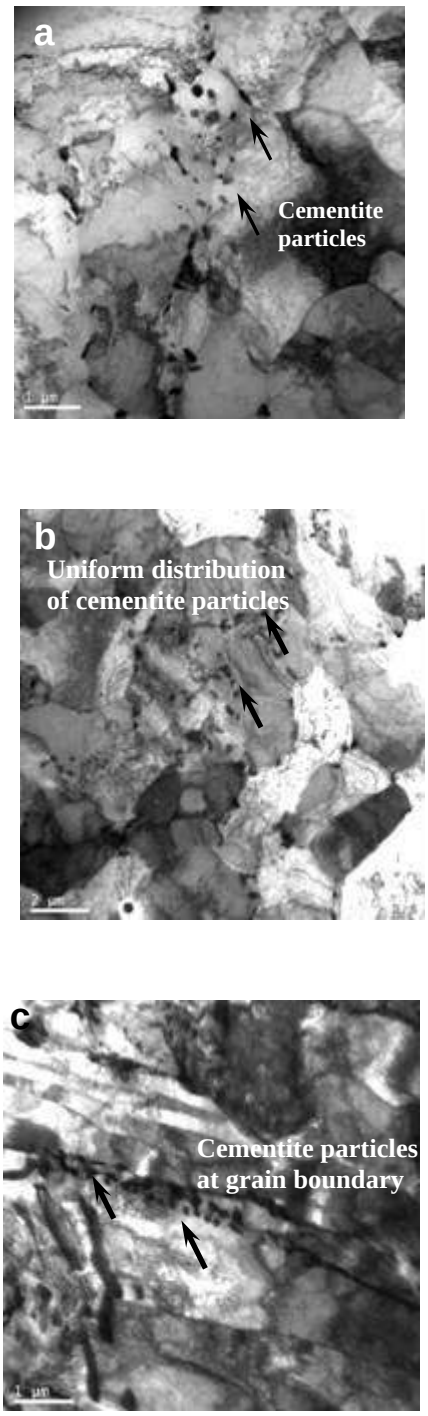

Figure 12. Bright field TEM micrographs of Nb-microalloyed steels processed at high cooling rate showing (a) cementite particles in ferrite (b) distribution of cementite particles in ferrite (c) cementite particles at the ferrite grain boundary [7].

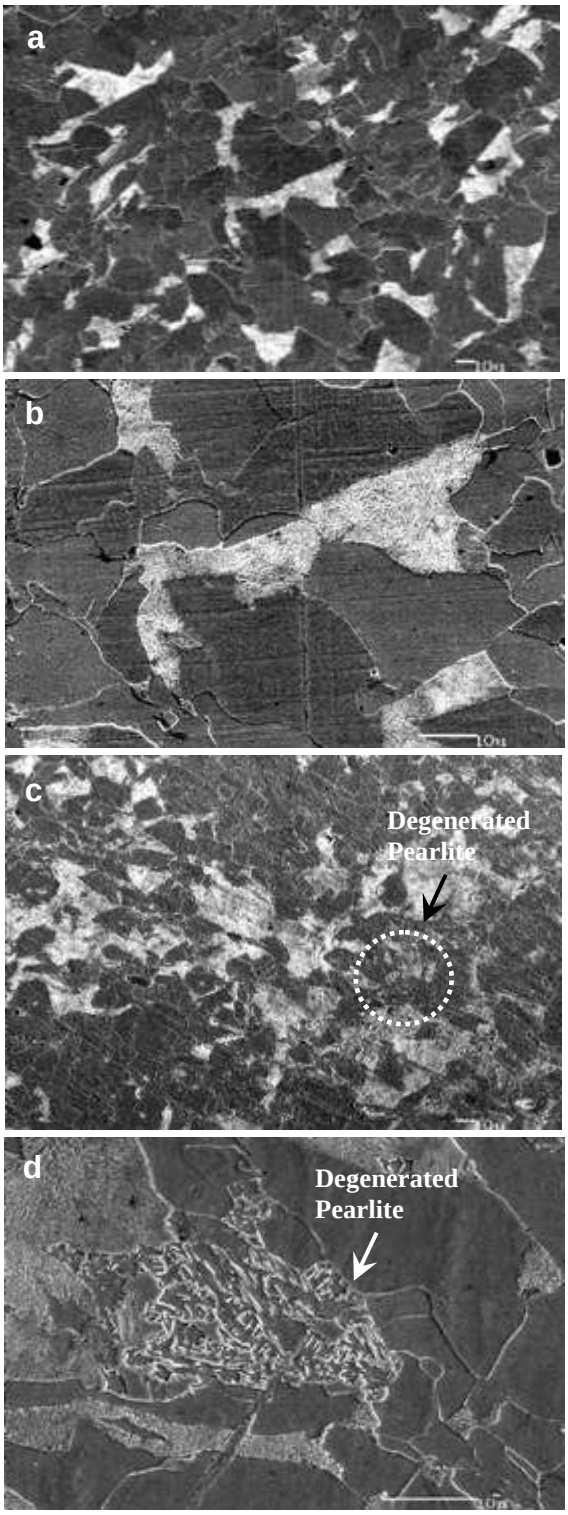

Figure 13. Representative low and high magnification scanning electron micrographs of V-microalloyed steel processed at (a, b) conventional and (c, d) high cooling rates. The micrograph (d) shows degenerated pearlite [7].

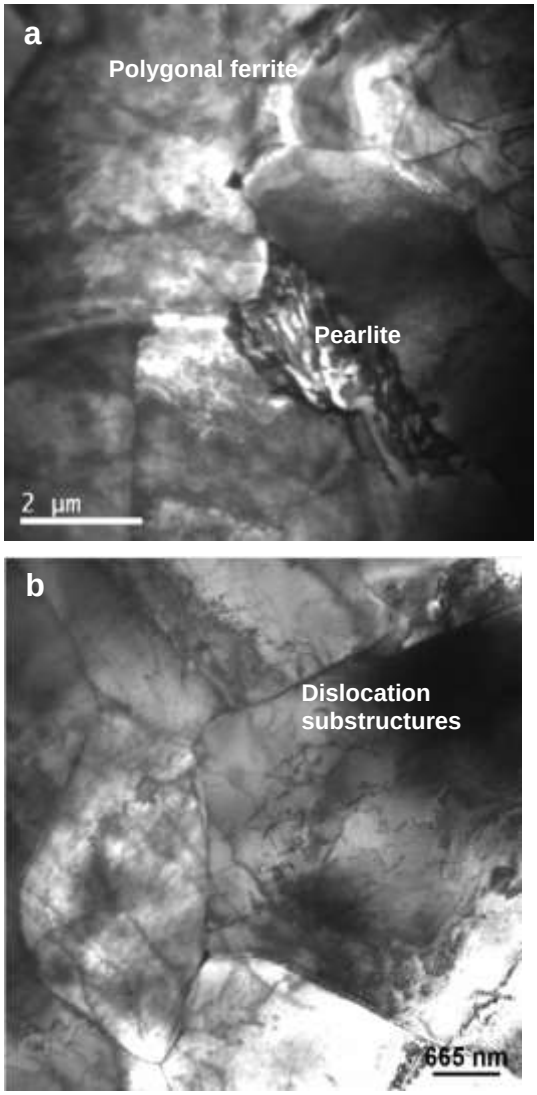

Figure 14. Bright field TEM micrographs of V-microalloyed steels processed at conventional cooling rate showing (a) polygonal ferrite-pearlite structure and (b) dislocation substructure in ferrite [7].

2.5. Precipitation in Nb- and V-Microalloyed Steels

Figure 16 (a,b) shows grain boundary precipitation and precipitation on dislocations in ferrite region of Nb-microalloyed steels, while Figure 17a shows precipitation in ferrite matrix together with the corresponding selected area diffraction (SAD) pattern in Figure 17b. The SAD pattern analysis indicated that the fine precipitates were MC type of cubic niobium carbides and the precipitates exhibited $[100]_{\square}//[110]_{NbC}$ Baker-Nutting orientation relationship with the ferrite matrix. Grain boundary precipitation and precipitation on dislocations in the ferrite region of V-microalloyed steels was also observed and is presented in Figure 18.

Figure 19a shows precipitation in the ferrite matrix of V-microalloyed steels and the corresponding selected area diffraction (SAD) pattern is shown in Figure 19b. In a manner similar to Nb-microalloyed steel, the SAD pattern analysis indicated that the fine precipitates were MC type of cubic vanadium carbides and the

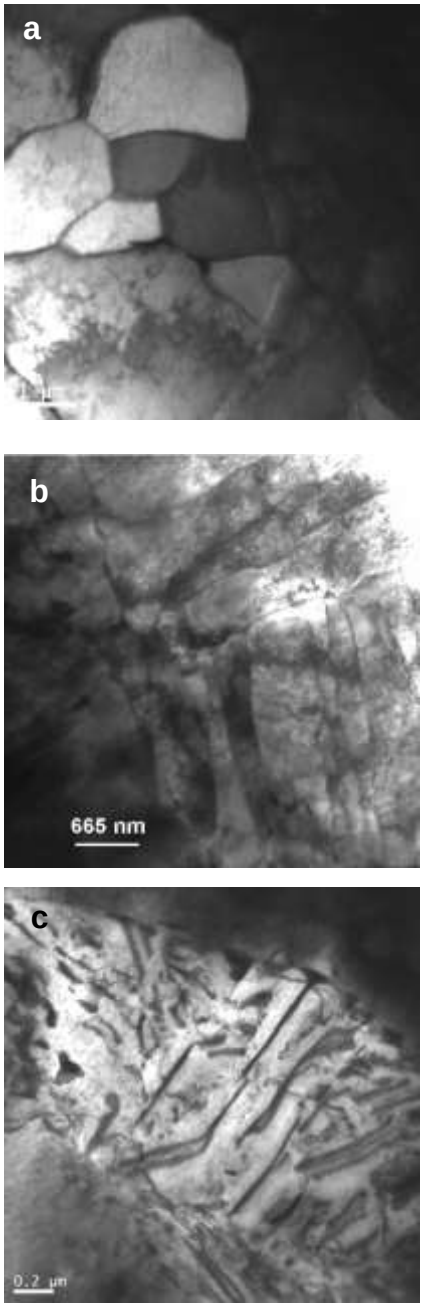

Figure 15. Bright field transmission electron micrographs of V-microalloyed steels processed at relatively high cooling rate showing (a) polygonal ferrite structure, (b) lath-type (acicular) ferrite structure, (c) degenerated pearlite [7].

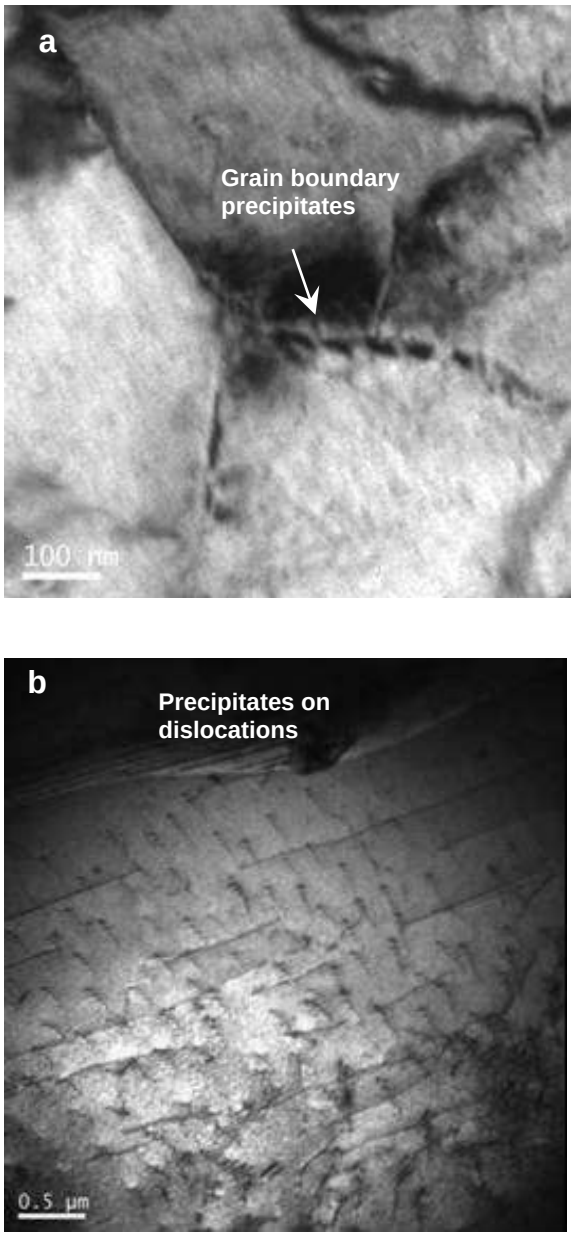

Figure 16. Bright field TEM micrographs of Nb-microalloyed steels showing (a) grain boundary precipitation and (b) precipitation on dislocations [7].

precipitates exhibited a cube-cube $[001]_{\alpha}//[001]_{VC}$ Baker-Nutting orientation relationship with the ferrite matrix. The characteristics of precipitates in terms of mean particle size, mean interparticle spacing and particle density in the matrix of both Nb- and V-microalloyed steels are summarized in Table III.

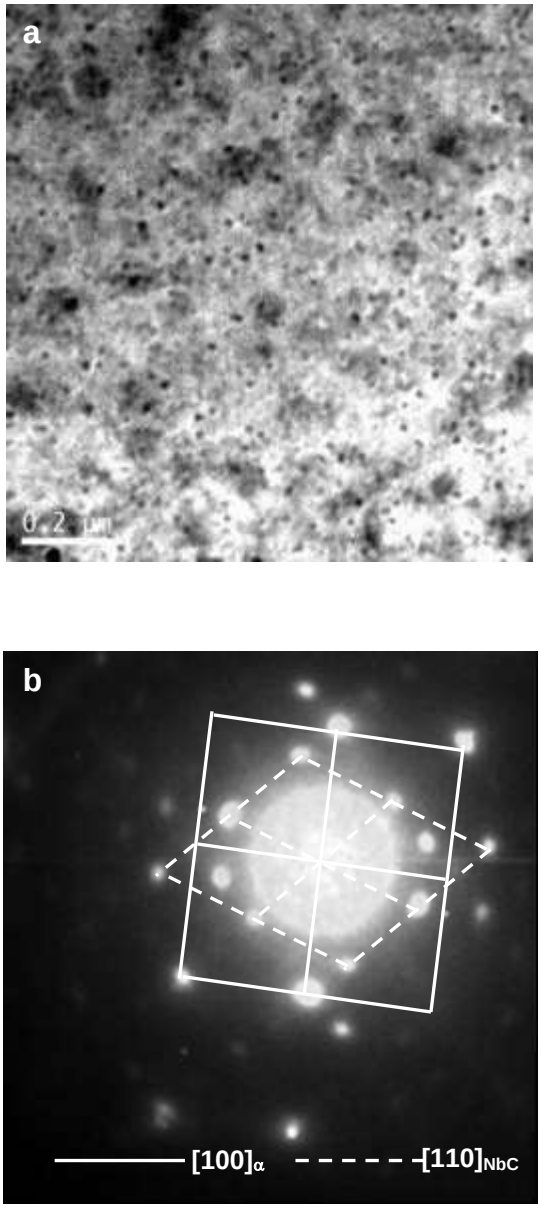

Figure 17. Bright field TEM micrograph of Nb-microalloyed steels showing (a) fine-scale precipitation in the ferrite matrix and (b) corresponding SAD pattern analysis for the precipitate and the matrix [7].

The above results suggest that Nb- and V-microalloyed steels experienced strain induced precipitation at grain boundaries, and dislocations, while the fine precipitates in ferrite formed during cooling. The precipitation of microalloying elements occurs during various stages of thermomechanical processing of steels. At soaking temperatures the

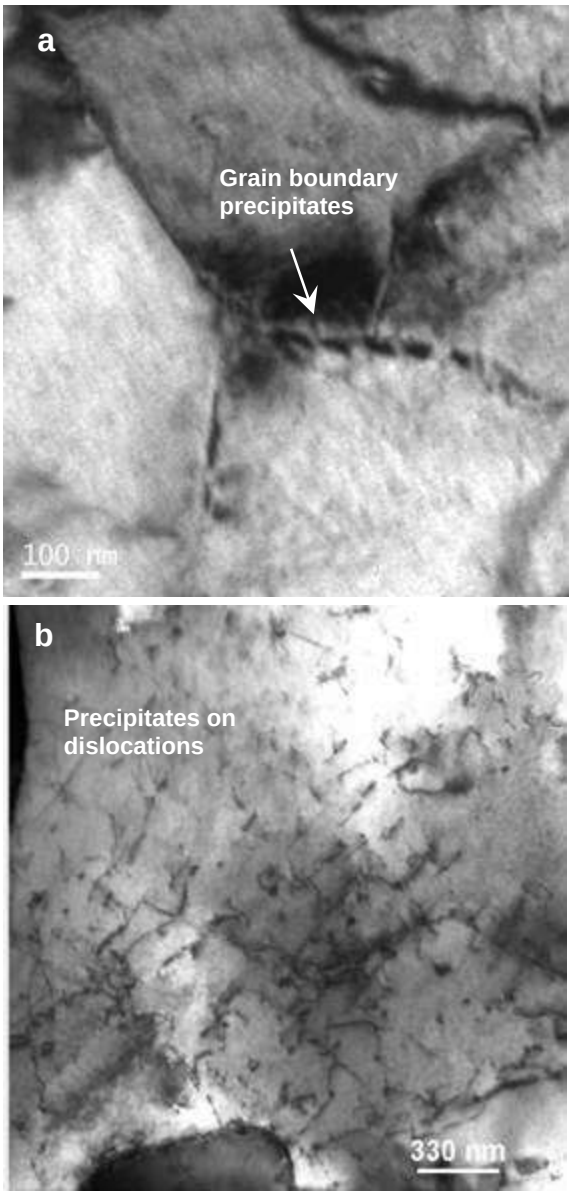

Figure 18. Bright field TEM micrographs of V-microalloyed steels showing (a) grain boundary precipitation and (b) precipitation on dislocations [7].

microalloying elements, Nb and V, are taken into solution depending on the limitation imposed by the solubility product. For carbide and nitride forming elements, the solubility in austenite at any given temperature depends on C and N content of the steel. When the temperature is lowered during cooling, supersaturation of these solute elements increases and precipitation begins at favorable kinetic conditions. Deformation of austenite introduce large amount of lattice defects such as dislocations and vacancies that assists the diffusional process that control the

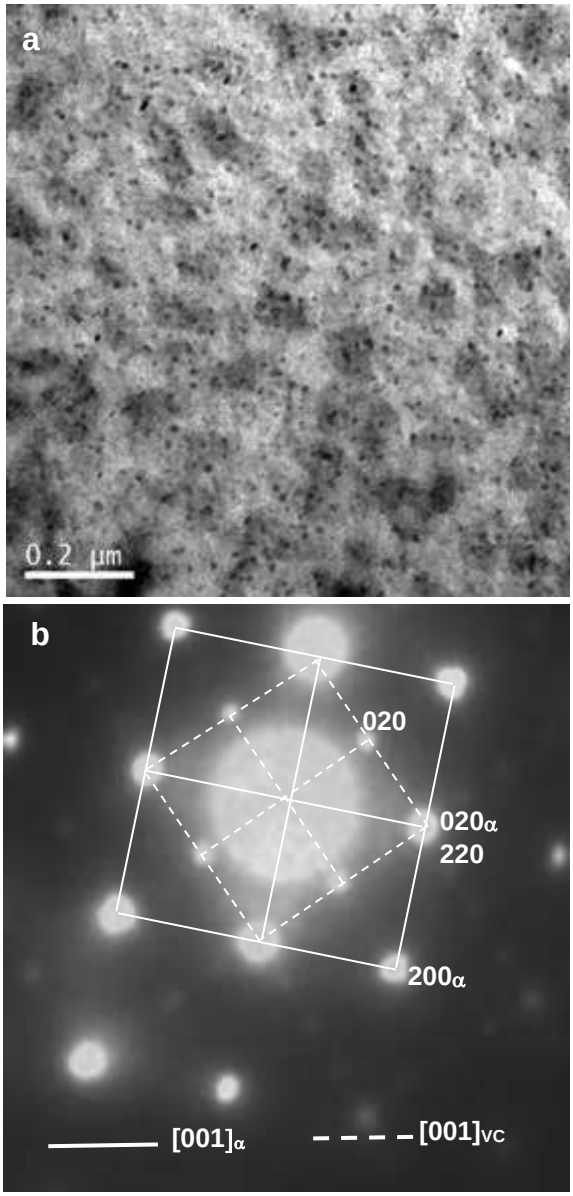

Figure 19. Bright field TEM micrograph of V-microalloyed steels showing (a) fine-scale precipitation in the ferrite matrix and (b) corresponding SAD pattern analysis for the precipitate and the matrix [7].

precipitation kinetics. As a result, strain induced precipitation occurs at the prior austenite grain boundaries or defects. In summary, the Nb- and V-microalloyed steels exhibited similar precipitation behavior in ferrite and the size range was from ~ 5 -10 nm (Table 3). It is reported that the effective size range for precipitation hardening is ~5-20 nm [14, 15]. These fine precipitates exhibited Baker-Nutting orientation relationship (Figures 17b and 19b) with the ferrite matrix of Nb- and V-microalloyed steels that may confirm that the precipitation occurred in ferrite.

Table 3. Precipitates Characteristics of Nb-and V-Microalloyed Steels

Properties	Nb-microalloyed steels		V-microalloyed steels	
	Convent-ional cooling rate	Higher cooling rate	Convent-ional cooling rate	Higher cooling rate
Mean particle size (d), nm	5.25 ± 3.5	7.5 ± 4.5	10.3 ± 4	8 ± 4.3
Mean inter-particle spacing, nm (50 measurements)	66 ± 37	50 ± 29	62 ± 31	44 ± 18
Particle density, (No. of particles/~ 0.5 μm^2)	280	320	210	375

2.6. Influence of Cooling Rate on Strength-Toughness Combination of Nb- and V-Microalloyed steels

The microstructural parameters that influence toughness are ferrite grain size, degenerated pearlite, and acicular ferrite/bainitic ferrite. The finer cementite in degenerated pearlite as compared to the conventional pearlite is expected to not only yield higher strength but also improves toughness because coarse pearlite deforms inhomogeneously with strain localized in narrow slip bands, where as fine degenerated pearlite exhibits uniform strain distribution during deformation [16]. Fine cementite particles also encourage the work hardening rate by creating the strain gradient near the particles due to the formation of Orowan loops. The dislocations constituting the strain gradient are referred as geometrically necessary dislocations [12, 13]. Thus, the significant increase in toughness with cooling rates of Nb-microalloyed steels is related to toughening enhancing phase, bainite.

3. Conclusions

Niobium as a microalloying element offers significant benefits in enhancing both strength and toughness of structural beams and plates. The benefits include refinement in grain size, precipitation strengthening and in obtaining strength-toughness

enhancing microstructure, notably bainite. Additionally, the effect of cooling rate on microstructure is more pronounced for Nb-microalloyed steels. In general, a higher level in strength and toughness is accomplished, when niobium is used as a microalloying element.

Acknowledgments

The author gratefully acknowledges financial support of CBMM-Reference Metals for the work presented here. Grateful thanks are also to Dr. D. Panda and Mr. T. Mannering for the industrial heats and helpful discussions.

References

1. I. Gonzalez-Bequest, R. Kaspar, and J. Richter, *Steel Research*, Vol 68**,** 1997, p61-66.
2. Q.Yu, Z. Wang, X. Liu and G. Wang, *Materials Science and Engineering A*, Vol 379, 2004, p384-390.
3. M. Charleux, W.J. Poole, M. Militizer and A. Deschamps, *Metallurgical and Materials Transactions A*, Vol 32, 2001, p1635-1646.
4. S. Jansto, Materials Science and Technology (MS&T) 2008, International Symposium on Materials Engineering for Structural Applications, October 5-9, 2008, p. 1289-1301.
5. L. Meyer, F. Heisterkamp, W. Muschenborn, *Micro Alloying*, 1975, p153-167.
6. M. Piette, E. Dubrulle-Prat, Ch. Perdix, V. Schwin, A. Streisselberger and K. Hulka, *Proceedings of The International Conference on Thermomechanical Processing of Steels*, May 24-26, 2000, London, UK.
7. S. Shanmugam, R.D.K. Misra, T. Mannering, D. Panda and S.G. Jansto, *Materials Science and Engineering A*, Vol 437**,** 2006, p436-445; and Vol 460-461**,** 2007, p335-343.
8. Y. Ohmori and R.W.K. Honeycombe, *Proceedings of ICSTIS (suppl.) Transactions Iron and Steel Institute of Japan*, Vol 11**,** 1971, p1160-1165.
9. G. Krauss and S.W. Thompson, *Iron and Steel Institute of Japan International*, Vol 35, 1995, p937-945.
10. Y. Ohmori, *Transactions Iron and Steel Institute of Japan*, Vol 11**,** 1971, p339-348.
11. T. Yamane, K. Hisayuki, Y. Kawazu, T. Takahashi, Y. Kimura, and Tsukuda, *Journal of Materials Science*, Vol 37, 2002, p3875-3879.
12. R. Song, D. Ponge and D. Raabe, *Scripta Materialia*, Vol 52**,** 2005, p1075-1080.
13. R. Song, D. Ponge, D. Raabe and R. Kaspar, *Acta Materialia*, Vol 53, 2005, p845-858.
14. R.D.K. Misra, G.C. Weatherly, J.E. Hartmann, and A.J. Boucek, *Material Science and Technology*, Vol 17, 2001, p1119-1129.
15. R.R. Thridandapani, S. Shanmugam, R.D.K. Misra, T. Mannering, D. Panda, and S. Jansto, *Proceedings of MS&T, 2005, TMS*, Pittsburgh**,** USA, p129.
16. H. Joung Sim, Y. Bum Lee and W.J. Nam, *Journal of Material Science*, Vol 39, 2004, p1849-1851.